RESEARCH ARTICLE

Periodicity of Single-Molecule Magnet Behaviour of Heterotetranuclear Lanthanide Complexes Across the Lanthanide Series: A Compendium

David Chukwuma Izuogu,*[a],[b],[c] Takefumi Yoshida,[b],[d] Goulven Cosquer,[e] Jonnie N. Asegbeloyin,[c] Haitao Zhang,[b] Alex J. W. Thom,*[a] Masahiro Yamashita*[b],[d],[f]

[a] Department of Chemistry, University of Cambridge, Lensfield Road, Cambridge, CB2 1EW United Kingdom
[b] Department of Chemistry, Graduate School of Science, Tohoku University, 6-3 Aza-Aoba, Aramaki, Sendai 980-8578, Japan
[c] Department of Pure and Industrial Chemistry, University of Nigeria, Nsukka, 410001, Enugu State, Nigeria
[d] WPI-Advanced Institute for Materials Research (AIMR), Tohoku University, 2-1-1 Katahira, Sendai 980-8577, Japan
[e] *Department of Chemistry, Graduate School of Science, Hiroshima University, 1-3-1 Kagamiyama, Higashihiroshima 739-8526, Japan*
[f] School of Materials Science and Engineering, Nankai University, Tianjin 300350, China

Supporting information for this article is given via a link at the end of the document.

Abstract: Acetato-bridged palladium-lanthanide tetranuclear heterometallic complexes of the form $(Pd_2Ln_2(H_2O)_2(CH_3COO)_{10})\cdot 2CH_3COOH$ (Ln_2 = Ce_2(**1**), Pr_2(**2**), Nd_2(**3**), Sm_2(**4**), Tb_2(**5**), Dy_2(**6**), $Dy_{0.2}Y_{1.8}$(**6''**), Ho_2(**7**), Er_2(**8**), $Er_{0.24}Y_{1.76}$(**8''**), Tm_2(**9**), Yb_2(**10**), Y_2(**11**)) were synthesised and characterised by experiment and theoretical techniques. All complexes containing the Kramers lanthanide ions (Ln^{3+}) (Ce (**1**), Nd(**3**), Sm(**4**), Dy(**6**), DyY(**6''**), Er(**8**), ErY(**8''**), Yb(**10**)) showed field-induced slow magnetic relaxation, characteristics of single-molecule magnetic and purely of molecular origin. In contrast all synthesised non-Kramers lanthanide ions (Ln^{3+} = Pr(**2**), Tb(**5**), Ho(**7**), Tm(**9**), Y^{3+}(**11**) is diamagnetic and non-lanthanide) did not show any slow magnetic relaxation. The variation in the electronic structure as well as accompany consequences across the complexes representing all Kramers and non-Kramers lanthanide ions were investigated. The origin of the magnetic properties and the extent to which the axial donor-acceptor interaction involving the lanthanide ions and an electron-deficient d_{z^2} of palladium affects the observed magnetic and electronic properties across the lanthanide series are presented. We report unique consistent electronic and magnetic properties of isostructural complexes spanning the lanthanide series with property variant dependent on whether the ions are Kramers or non-Kramers.

Introduction

Lanthanide-based Single-molecule magnets (SMMs) have shown great promise in the realisation of quantum information processing[1] due to the bistability nature of their spin(s) coupled with strong magnetic anisotropy.[2–4] As frontiers in molecule-based magnets continue, recent results have proven the need to fully understand the structural information of magnetic materials and how they affect observed slow magnetic relaxation. For a long time, one of the fundamental considerations in the construction of SMMs was based on the maximisation of the total spin in the ground state(S). However, some results which showed transition metal clusters with total high spin states but small effective energy barrier (U_{eff}) and low blocking temperature (T_B) questioned this consideration.[5,6] A large U_{eff} means that the *S* must be maximised without interactions that cancel the intrinsic magnetic anisotropy, a property which is best observed with lanthanide-based complexes due to strong spin-orbit interaction, making lanthanide (Ln) best suited for quantum devices fabrication.[7,6] The axial zero-field splitting(*D*) parameter would need to be large and negative for SMMs with high T_B to allow for the magnetic sub-level with the largest magnetic moments to be lowest in energy. Attempts aimed at maximising *S* by incorporating many transition metal centres in clusters tend to produce an overall *S* and *D* – values that do not improve the SMM behaviour of the system under investigation.[6,8] In the case of Ln-based SMMs, *D* and S has shown to be nearly independent, due to spin-orbit coupling leading to a large intrinsic *D* and *J* values (from the m_J-states) for a single ion, compared to a transition metal. The sensitivity of the magnetic property of Ln-based SMMs to ligand variations opens the avenue for in-depth research to understanding the structural information required to obtain enhanced SMMs materials. Such structural variations have led to interesting advances in the observation of SMM behaviour using metal-metal bonding interactions, peripheral ligand modifications, organometallics lanthanide-based complexes as well as multiple deckers complexes.[2,3,9–13] Recent advances have proven lanthanide-based complexes to show better promise in the journey to realising close to liquid nitrogen SMM materials.[3,4,14–16] Attempts have also been made to incorporate magnetic[17–19] and nonmagnetic[20–23] transition metals in molecular lattices of lanthanide complexes, but not in ways of any form of polarisation or electron density donation to the lanthanide centre. As a result of the progress made so far in lanthanide-based SMM, this work is focused on understanding more about the factors that inhibit or promote SMM behaviour in lanthanide complexes. There has

been much work on how factors, like symmetry, peripheral ligand substitution, and nature of donor atoms affects SMM behaviour.[24,25,26,27] Attempts has also been made to oxidise/reduce complexes[28], introduce heteronuclear magnetic centres[20–23] in other to enhance SMM behaviour. The intrinsic quadrupole moment approximation of *f*-orbitals which divides the lanthanide ions into oblate and prolate electron distribution allows to rationally induce some level of anisotropy more efficiently than for transition metals. The spin-orbit-coupled ground state leading to the bistability arising from the 2*J*+1 microstate means that one can expect a much larger magnetic moment for Ln-based SMM. Coordination factor such as donor character of the ligand, the proximity of the donor atoms to the magnetic lanthanide centre, coordination angle, charge of the donor atom and the nature of the donor atoms have become important tools in the design of enhanced SMM materials. Although *f*-electrons are deeply rooted in the core-shell, their energies are slightly affected by the ligand field, which affects their magnetic properties. Consequently, different magnetic behaviour can be accessed by affecting the *f*-electron cloud with variations in the ligand field. Molecular designs that place two lanthanide centres next to each other can induce *f*-*f* interactions which can affect SMM properties by enhancing it or in most cases, induce quantum tunnelling of magnetisation (QTM) that speeds up relaxation and degrades SMM behaviour, as demonstrated by multiple-decker complexes.[29–36] As a result of the core character of *f*-electrons, they have a tiny contribution in the formation of bonds which explains the scarcity of homo Ln – Ln bond. However, it has been shown that transition metals like Pt^{2+} and Pd^{2+} could donate some electron density to a lanthanide centre, with implication to the magnetic property of the complexes.[9,12,37,38,39] Pt^{2+} was favoured for a higher electron donation over Pd^{2+} due to the more radially extended $5d_{z^2}$ orbital of platinum that readily pushes more electron density compare to the $4d_{z^2}$ of palladium.[39] Yoshida *et al.* also showed that such Pt-Ln hetero-bond has significant effect not only on the magnetic properties but also in the luminescence.[9] Kramer's ions can show slow magnetic relaxation which is field-dependent as a manifestation of electronuclear spin entanglement.[40,41] The large unquenched orbital momentum, magnetic anisotropy, and large m_J - value for single ion made lanthanide ions good candidates for the construction of SMMs. There is constant but sometimes confusing evidence on the importance of symmetry and geometry in determining whether a compound would show SMM behaviour or not.[39,42–45] This is because symmetry and geometry alone are not the sole determinants of SMM property. The present study deals with the slow magnetic relaxation for the lanthanide series of Pd-Ln-Ln-Pd acetate bridged complexes (where Ln= Ce, Pr, Nd, Sm, Tb, Dy, Ho, Er, Tm, Yb, and Y). La and Lu were not investigated for lack of unpaired *f*-electron spin, Eu and Pm were avoided because of a spin-orbit coupling value of zero and radioactivity respectively while Gadolinium(Gd) will be referenced from a previous report.[13] We present how axiality, symmetry, quadrupole moment approximation, splitting of Kramers doublets and electron-density donation combine to determine the electronic state of a complete series of Ln-based complexes. We investigated the series to show trends in the observed electronic and magnetic properties.

We show with convincing evidence that the discrepancy observed in the slow magnetic relaxation of all the Kramer's doublets over the non-Kramer's doublets of the Pd-Ln-Ln-Pd series stems from the extent of electron density donation from the palladium and oxygen donors and rationalises the observed phenomena with previous reports containing platinum and sulphur donors.

Results and Discussion

13 isostructural complexes, general formula $(Pd_2Ln_2(H_2O)_2(CH_3COO)_{10})\cdot 2CH_3COOH$ (Ln_2 = Ce_2(**1**), Pr_2(**2**), Nd_2(**3**), Sm_2(**4**), Tb_2(**5**), Dy_2(**6**), $Dy_{0.2}Y_{1.8}$(**6"**), Ho_2(**7**), Er_2(**8**), $Er_{0.24}Y_{1.76}$(**8"**), Tm_2(**9**), Yb_2(**10**), Y_2(**11**)) were synthesized. Eu^{3+}, Lu^{3+} and Pm^{3+} were not investigated because they respectively have a *j*-value of zero, possesses a total spin state of zero and is radioactive. **6"** and **8"** are diamagnetically diluted samples of **6** and **8** using Dy:Y and Er:Y in the ratio of 0.20 : 0.80 respectively (see experimental section of supporting information and Table S1). The crystal structure has been described in the previous structural reports of **3**, **9**, **10**, **11** and **Pd-Gd** congeners.[13,46] **1**, **2** and **4** will not be described due to difficulties in obtaining a single crystal structure and so isostructural identity was only determined using powered X-ray Diffraction as presented in Figure S1. Therefore, only a brief description of **6** will be given here as a representative structure with focus on differences that underpinned the observed electronic and magnetic properties of the lanthanide series presented. Figure S2a shows the crystal structure of **6** obtained at room temperature as a monoclinic space group $P2_1/n$ while the crystallographic data of selected complexes are shown in Table S2. The molecular structure is made up of two asymmetric units bridged together by two acetato ligands. The asymmetric unit (Figure S2b) is made up of a palladium ion bridged to a dysprosium ion by four bidentate acetato ligands to form a cage-like pocket between Pd^{2+} and Dy^{3+} with a Pd-Dy interaction which gives the palladium a total coordination number of five in a square-pyramidal fashion. The dysprosium centre is then further coordinated to a water molecule

and two acetato ligands which bridge the two asymmetric units. Each of the two asymmetric units bridging acetato is coordinated to one dysprosium via a monohapto (η^1) oxygen and the other dysprosium via a dihapto (η^2) oxygen in which the η^2-oxygen in each acetate serves as the bridge. This brings the coordination number of the dysprosium centre to nine. The two asymmetric units linked through the bridging acetato ligand form a paddle-wheel structure of our heterotetrametallic complex. There is an interesting trend in the Pd-Ln as well as the intermolecular Ln-Ln distances (Figure S3 and Table 1) as you move across the period of the lanthanide series depending on whether the lanthanide ion is a Kramers ion or not. Generally, the effective nuclear charge increase across the period from cerium to lutecium should have a corresponding decrease on the ionic radius leading to shorter Ln-Ln distances (Table 1). However, the Pd-Ln distances (Table 1) did not follow a smooth trend as the Ln – Ln distances due to the different level of bonding interaction between the palladium ion and the lanthanide as will be presented later under the molecular orbital diagram from TDDFT.

Table 1. Intramolecular Pd-Ln and Ln – Ln as well as intermolecular Ln – Ln distances of some selected isostructural complexes (compounds **3**, **5**, **6**, **7**, **8**, **9**, **10, 11** and **Pd-Gd**)

Complex	Pd-Ln (Å) [a]	Ln-Ln (Å) [a]	Ln-Ln (Å) [b]
Pd-Y (11)[13], [b]	3.195	4.034	8.491
Pd-Nd (3)[46]	3.221	4.172	8.677
Pd-Gd[13]	3.195	4.089	8.557
Pd-Tb (5)	3.190	4.050	8.490
Pd-Dy (6)	3.191	4.039	8.475
Pd-Ho (7)	3.191	4.023	8.458
Pd-Er (8)	3.189	4.006	8.445
P-Tm (9)[46]	3.178	3.992	8.415
Pd-Yb (10)[46]	3.183	3.982	8.408

[a] Intramolecular. [b] Intermolecular. [c] Not Ln but included for its use in diamagnetic dilution in magnetic measurements.

The existence of two asymmetric units in the molecule consequently created an inversion centre (Figure S4a) at the middle of the 4-sided ring created by the bridging acetato ligands giving the entire molecule a symmetry label of C_i which can alternatively be viewed as a 2-fold axis of improper rotation S_2 as depicted in Figure S4b. However, considering the first coordination sphere of **6**, we found that the Dy^{3+} and all other isostructural motifs presented in this paper are in the same distorted D_{3h} tricapped trigonal prism as previously reported for an isostructural Pd-Gd compound.[13]

Absorption spectra and Electronic structure Theory

Liddle *et al.* had shown that spectroscopic investigations are prerequisite for an in-depth understanding of SMM behaviour due to their role in determining the electronic structure of such systems exhibiting SMM behaviour.[47] Although, a Pd-La model isostructural to the family of complexes currently under investigation has been used to probe the various excited states observed in gadolinium congener,[13] we observed that the absence of *f*-electrons in La^{3+} might have led to the loss of some vital information necessary to describe a complete picture of actual lanthanide complexes with *f*-electrons. The Pd-Dy (**6**) complex was therefore chosen as a representative of lanthanide with *f*-electrons. The time-dependent density functional theory (TDDFT) calculation was carried out using the crystal structure measured directly from X-ray diffraction without optimisation to ensure that the structural integrity is not compromised. The calculation details are provided in the supporting information. The TDDFT result reproduces the solid-state UV-VIS spectra for **6** (**Figure 1**).

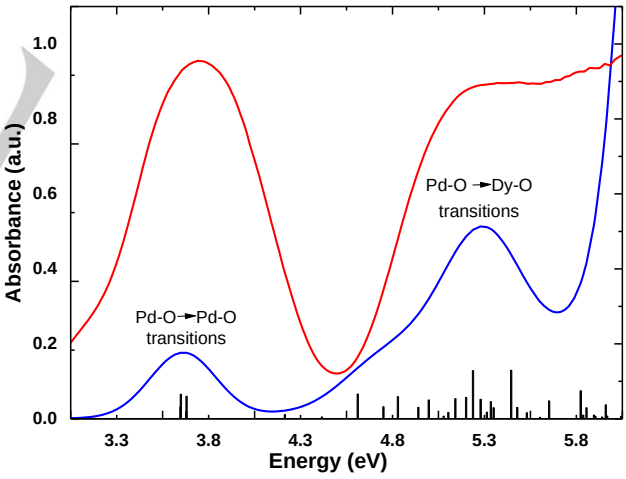

Figure 1. Absorption spectra for **6** (red line: experimental) in solid-state with $BaSO_4$ background and calculated (Blue line) from TDDFT in a vacuum.

Two absorption maxima were observed in the visible region at 3.70 eV (354.24 nm) and 5.26 eV (235.71 nm). The two maxima are in accordance with previous report[13] except for the molecular orbitals type involved in the absorption. The energy of maximum absorption (for the experiment in Figure 1) was calculated as 3.60 eV (344.40 nm) which approximately matches both our previous report (3.66 eV or 338 nm) and experimental value (3.70 eV or

354.24 nm) obtained using complex **6**. The absorption maxima in Pd-La was attributed to the transition from the highest occupied molecular orbital (HOMO) whose identity was shown to be the Pd-La molecular orbital to the lowest unoccupied molecular orbital (LUMO) with a predominant $d_{x^2-y^2}$ orbital character of the palladium ion. The lack of unpaired electrons in the Pd-La model means that the alpha (α) and (beta) β orbitals have equal contribution to the overall HOMO. For the Pd-Dy (**6**) system which possesses unpaired electron spins, the case is different, and so, we show the different α and β orbital occupancy mainly for the set of orbitals involved in the observed transition in the visible region (Table S3) to clarify our adoption of α and β HOMO and LUMO terms in describing the observed transitions as shown below.

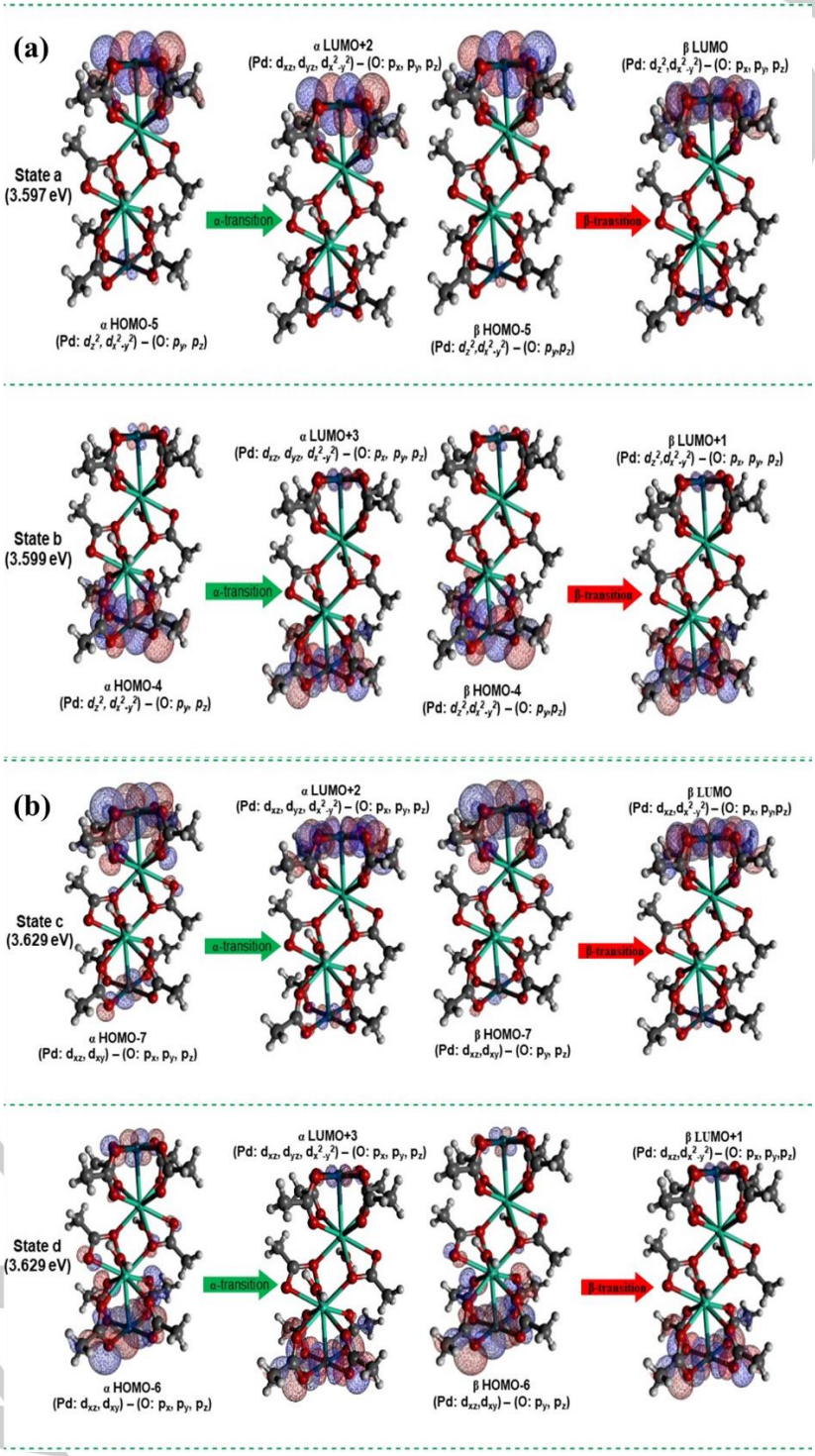

Figure 2. Molecular orbital mapping for complex 6 showing orbital contributions to the transitions (a) at about 3.597 and 3.599 eV at states a and b from TDDFT (b) at about 3.629 at states c and e eV from TDDFT (green arrow: α-transitions; red arrow: β-transitions)

Interestingly, the TDDFT result for **6** shows that while the Pd-Dy orbital interaction exists as the HOMO (α or β) (Figure S5), the absorption maximum does not originate from the HOMO nor end up at the LUMO (α or β) (Figure 2).

We observed a range of transition which are a linear combination of contributions from various molecular orbitals predominantly Pd^{2+} d – O^{2-} p-orbitals as shown in states a – d of Figure 2. The transitions span both the α and β space with the α space involving αHOMO-4, αHOMO-5, αHOMO-6 and αHOMO-7 to αLUMO+3, αLUMO+2, αLUMO+3 and αLUMO+2 transitions respectively while the β space comprises of transitions from βHOMO-4, βHOMO-5, βHOMO-6 and βHOMO-7 to βLUMO+1, βLUMO, βLUMO+1 and βLUMO respectively. We attributed the discrepancies in the molecular orbital from which the transitions originated when compared to the Pd-La to the stronger Pd-Dy interaction arising from a slight increase in the effective nuclear charge on moving from $_{57}$La to $_{66}$Dy as well as the occupation of *f*-orbitals in dysprosium. Consequently, transitions involving electrons in the α-space with energy spacing corresponding to the triggered transitions in the β-space were then observed in favour of HOMO – LUMO transitions as observed for Pd-La. This result is in accordance with the decreased tendency of HOMO-LUMO transition occurring in the visible region when compared with the $Pd_3(CH_3COO)_6$.[13]

The Pd-La model showed that the LUMO was concentrated on the Pd $d_{x^2-y^2}$ orbital, in contrast, the (α + β)LUMO (Figure S5) for Pd-Dy (complex **6**) from the TDDFT shows the LUMO to be hybrid orbitals of Dy^{3+} s, $f_{z(x^2-y^2)}$, and $f_{x(x^2-3y^2)}$. Transitions to the αLUMO from αHOMO-5, αHOMO-7, αHOMO-14, αHOMO-15, αHOMO-16 and αHOMO-17 dominates the second broad absorption peak in the absorption spectra with little contributions from αHOMO-4 and αHOMO-17 to αLUMO+1 (Figure S6, S7 and S8) This is a further confirmation of the different energy separation between the (α + β)LUMO and their respective (α + β)HOMOs when compared to Pd-La. Each state shown in Figure 2 and S6 – S8 is represented by the thread peak in the TDDFT spectra (Figure 1). The electron-electron interaction energies are usually higher (order of magnitude of about 13 eV, 100,000 cm^{-1}, 100 nm) compare to the spin-orbit and ligand-field interactions which have made lanthanide-based complexes prime candidates for SMM design. It might be possible to trace the origin of various transitions to the magnitude of ligand-field and spin-orbit coupling energies as absorbed energies are converted or redistributed within a given molecular system. In future, we will be looking into how to extract more meaningful information from absorption spectra and its relationship to magnetic properties of molecular magnets using theoretical methods.

Static Magnetic Properties

The static magnetic properties were carried out using their corresponding polycrystalline powder whose phase purity was ascertained before measurement by obtaining their powder X-ray diffraction (PXRD) patterns (Figure S1).

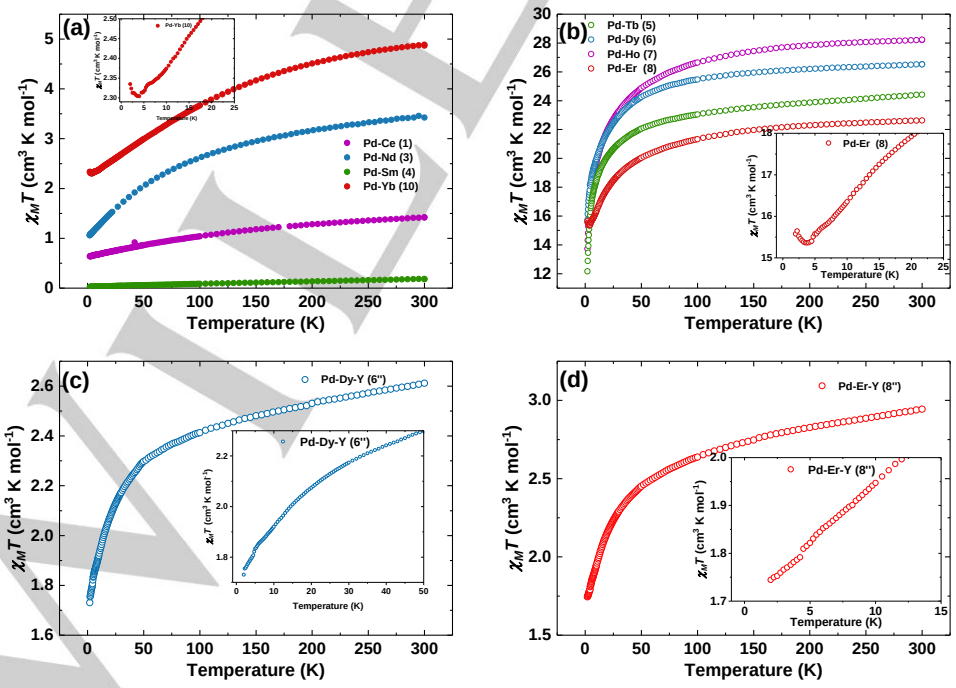

Figure 3. $\chi_m T$ versus *T* plot for (a) **1, 3, 4** and **10** (inset: maximised plot of **10** at temperature range of 2 – 20 K) (b) **5**, **6**, **7** and **8** (inset: maximised plot of **8** at temperature range of 2 – 20 K) (c) **6''** (inset: maximised plot of **6** at temperature range of 2 – 50 K) (d) **8''** (inset: maximised plot of **8''** at temperature range of 2 – 15 K) (all measurements were carried at *dc*-field of 1000 Oe).

The PXRD pattern of all polycrystalline samples used for all magnetic measurements matched the simulated pattern obtained from the single-crystal X-ray diffraction, confirming the phase purity of all isostructural congeners. By applying a direct current (*dc*) field of 1000 Oe, the static magnetic susceptibilities of the samples were obtained in the temperature (*T*) range 2 – 300 K (Figure 3).

The $\chi_m T$ values for all measured samples tend to follow a general downward slope as the temperature is decreased. The $\chi_m T$ values at room temperature (RT) are close to the corresponding $\chi_m T$ values of two uncoupled free lanthanide ions (Figure 3a and 3b and Table 2).[48,49]

Table 2. Comparison of experimental and theoretical $\chi_m T$ values for **1**, **3**, **4**, **5**, **6**, **7**, **8**, and **10** at Room temperature and 2 K.

complex	Experimental χ_mT @ 2 K (cm^3Kmol^{-1})[a]	Experimental χ_mT @ RT (cm^3Kmol^{-1})[a]	Theoretical χ_mT @ RT[48,49] (cm^3Kmol^{-1})[a]	Ln^{3+}	Spin-orbit parameter
1	0.64	1.42	1.60	Ce^{3+}	(S=1/2, L=3, $^2F_{5/2}$, g=6/7)
3	1.05	3.42	3.28	Nd^{3+}	(S=3/2, L=6, $^4I_{9/2}$, g=8/11)
4	0.02	0.17	0.18	Sm^{3+}	(S=5/2, L=5, $^6H_{5/2}$, g=2/7)
5	12.16	24.40	23.64	Tb^{3+}	(S=3, L=3, $^7F_6$, g=3/2)
6	15.73	26.98	28.34	Dy^{3+}	(S=5/2, L=5, $^6H_{15/2}$, g=4/3)
7	13.71	28.20	28.14	Ho^{3+}	(S=2, L=6, $^5I_8$, g=5/4)
8	15.36	22.63	22.96	Er^{3+}	(S=3/2, L=6, $^4I_{15/2}$, g=6/5)
10	2.33	4.90	5.14	Yb^{3+}	(S=½, L=3, $^2F_{7/2}$, g=8/7)

[a] values are for two uncoupled Ln^{3+}.

For complexes **5**-**8**, the $\chi_m T$ remains relatively constant with a decrease in temperature from *RT* until about 100 K before decreasing noticeably. The same decrease can be observed for complexes **1**, **3**, **4** and **10** in a more steady but gradual manner. These decreases could be attributed to a possible thermal depopulation of the crystal-field-split magnetic levels (M_J states) or destructive intramolecular magnetic coupling (antiferromagnetic interaction) between the two closely bridged lanthanide ions as described in the crystal structure section. However, the shortest Ln-Ln inter- or intra- molecular distances (Table 1) are too long to allow magnetic coupling between the magnetic centres and so we overrule the possibility of an intermolecular magnetic coupling as the *f*-electrons are deeply localised within the core-shell of lanthanide ions.[36,50] This leaves the thermal depopulation of the m_j levels as the main reason for the observed decrease in the $\chi_m T$. Complexes **8** and **10** show slight increase in the magnetic susceptibility value (inset of Figure 3b and 3a) below 5 K. We attribute this observation to the shorter Ln-Ln intramolecular distances observed for **8** and **10** (Table 1) which allowed ferromagnetic coupling below 5 K. To confirm this, a diamagnetic diluted sample of **8** (**8''**) have been synthesised using 88.2 % of diamagnetic yttrium ion for its preparation. The dilution ensured that Er-Er bridges are not formed within one molecule as well as eliminates possible intermolecular dipole-dipole interaction within the crystal lattice. The observed increase in $\chi_m T$ value of **8** disappeared in **8''** (inset of Figure 3d), confirming a possible intramolecular ferromagnetic coupling between the two bridged Er-Er magnetic centres below 5 K. The effective nuclear charge which increases across the period from lanthanum to lutetium causes the Ln-Ln distance to shorten, allowing a stronger attraction between the lanthanide centres for erbium and ytterbium complexes.

As a consequence, the loss of thermal energy below 5 K causes a ferromagnetic interaction to dominate over depopulation of the m_j levels compare to other congeners with lesser effective nuclear charge (Ce^{3+} – Ho^{3+}) and therefore longer Ln-Ln distances. The proximity of the Ln-Ln centres coupled with the electron density distributions (the quadrupole moment approximations) was confirmed to play a significant role in the magnetic properties of the lanthanides.[7,48]

The magnetisation *vs* field for **5**, **6** and **8** shows usual magnetic saturation for terbium, dysprosium and erbium ions respectively (Figure S9), with a small butterfly type hysteresis opening, typical of SMM behaviour, for complex **5**. We do not observe this slight opening for other members of the lanthanide series investigated. **5**, therefore, functions as a paramagnet.

One of the significant ways to ascertain the level of magnetic anisotropy apart from EPR measurement is the plot of

magnetisation versus the product of field and reciprocal of temperature (*M vs* HT^{-1}). An isotropic system would show an overlaid lines against temperature variants whereas, a deviation from this would mean some degree of magnetic anisotropy of the system. Complexes **6** and **8** (Figure 4b and 4c) shows a significant degree of magnetic anisotropy characteristics of SMM behaviour as would be expected given the intrinsic single-ion anisotropy of Dy^{3+} and Er^{3+}. Although neodymium-based magnets are most widely used permanent magnets, they have not found a place in the development of SMM.

If the exceptional strong permanent magnetism of neodymium can be exploited in SMM design, it could be the beginning of the development of a new class of room temperature SMMs. The *M* vs HT^{-1} plot of both **3** and **10** shows an appreciable degree of magnetic anisotropy (Figure 4a and 4d). This has made the present study a significant contribution to the development of SMMs. The magnetic anisotropy, which impacts significantly on the spin relaxation, is attributed to the unprecedented electron density donation from the d_{z^2} orbital of the electron-deficient palladium ion to the hybrid frontier orbitals of the lanthanide ions.[39,13]

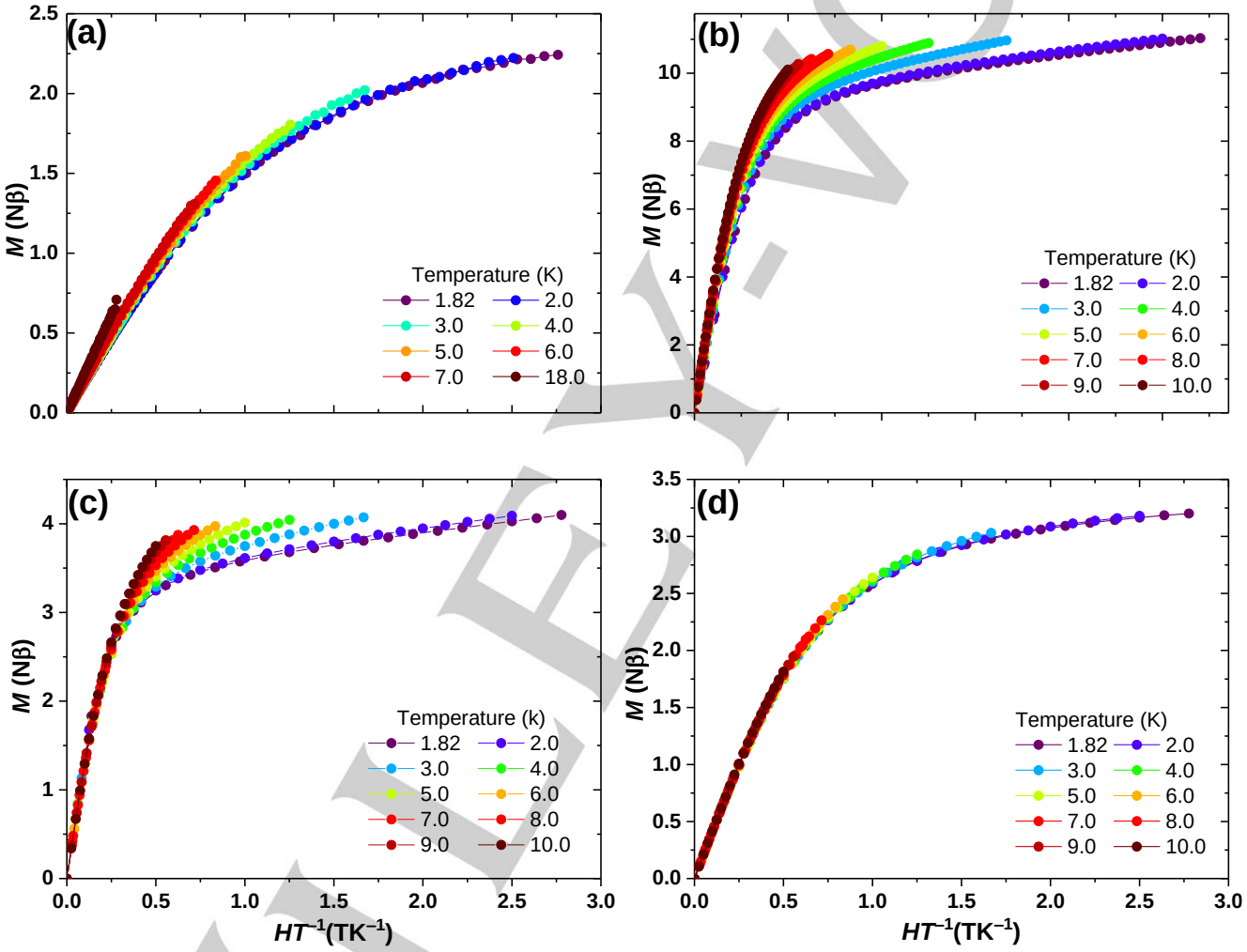

Figure 4. *M* vs HT^{-1} plots for (a) complex **3** from 1.82 – 18 K (b) complex **6** from 1.82 – 10 K (c) complex **8** from 1.82 – 10 K and (d) complex **10** from 1.82 – 10 K.

Dynamic Magnetic Properties

The alternating current (*ac*) susceptibility measurement was carried out using the same polycrystalline samples with confirmed phase purity as in the case of *dc* measurement. We carried out *ac* susceptibility measurement for all isostructural lanthanide complexes (complexes **1** – **10**) of the Pd-Ln system under investigation, except for Gd^{3+}, which was previously investigated.[13] Obtained results showed that all the systems with Kramers ions (Ce (**1**), Nd(**3**), Sm(**4**), Dy(**6**), DyY(**6''**), Er(**8**), ErY(**8''**), Yb(**10**)) showed frequency-dependent slow magnetic relaxation characteristic of SMM behaviour under applied *dc* magnetic field. The ground state *J* multiplet of the Kramers ions splits into several sub-states that are characterised by the J_z

quantum number. Considering, for example, a Dy^{3+} $^6H_{15/2}$ ground-state multiplet, the energy could be represented by equation 1.[51]

$$E(J_z) = 3B_2^0 J_z^2 + B_4^0\{25J_z^4 - 30J(J+1)J_z^2 + 25J_z^2\} + B_6^0(231J_z^6 + polynomial\ of\ J_z^4, J_z^2, and\ J \quad \text{_____} 1$$

B_n^m is the crystal field anisotropy parameter. On the other hand, all synthesised non-Kramer's lanthanide ions (Pr (**2**), Tb(**5**), Ho(**7**), Tm(**9**)) did not show slow magnetic relaxation (Figure S10). This is an improvement compared to previously reported Pt-Ln system which does not have such a clear division between Kramers ions and non-Kramers ions.[9,12] Such clear cut among the lanthanide series makes it more exciting and convenient to investigate the precise mechanism and factors leading to the observed slow magnetic relaxation in lanthanide-based molecular magnets.

Complexes based on Ce, Nd, Sm, and Yb are rarely reported as SMM compared to Dy or Tb based complexes. Notable examples are found in the review by Pointillart *et. al.*[52] and the references therein. To the best of our knowledge, there has been no report on samarium-based complex showing slow magnetic relaxation. Our literature search reviewed that samarium based complexes have been well studied for luminescence as shown in reference 53 and references therein but not for slow magnetic relaxation.[53] Complexes **1**, **3**, **4**, and **10** (respectively based on Ce, Nd, Sm, and Yb) shows slow magnetic relaxation, characteristic of SMM behaviour, under various magnetic fields, at 1.85 K for complexes **1** and **10** and 2 K for complexes **3** and **4** (Figure S11 and S12). Without the magnetic field, slow magnetic relaxation was not observed for **1**, **3** and **10**. This is attributed to the very fast magnetic tunnelling in the absence of field due to intermolecular dipole-dipole interactions.[54–56] On the other hand, **4** shows slow magnetic relaxation with and without applied *dc* field. The peak top, however, lies beyond the measured 1500 Hz of our instrument at all field. **10** shows two relaxation time, a slower one at about 0.1 – 1 Hz and the primary process with peak top around 100 Hz. The optimum observed field (field with the highest recorded intensity for the out-of-phase signal peak) (Figure S13) is then used for a temperature scan for the corresponding complex at a fixed field.

The field scan at 1.85 K for **6**, **6''** and **8**, and 2 K for **8''**, shows slow magnetic relaxation under applied *dc* field (Figure S14 and S15). Complexes **6** and **8**, respectively based on Dy^{3+} and Er^{3+}**,** show optimum fields of 2000 Oe and 800 Oe respectively. It is important to state that the optimum fields were used for the temperature scans rather than a specified field for all complexes which could allow extraction of relaxation trend at that field because of the interest in investigating the slowest relaxation dynamics across the series for the highest magnetic responses (out-of-phase magnetic susceptibility) irrespective of the field. The diamagnetic diluted samples, **6''** and **8''** retains the slow magnetic relaxation with a slower relaxation time compared to **6** and **8** respectively. This confirms the absence of spin-lattice relaxation in both our pure and diluted samples sometimes observed in most gadolinium and vanadium complexes.[57,58,45] Besides, complexes **6** and **6''** shows slow magnetic relaxation without magnetic field. **8** does not show slow magnetic relaxation without field while **8''** showed a feeble response at very high frequency. The difference between pure and diamagnetically diluted samples is attributed to the suppression of the intra- or inter- molecular interaction, which induced a diminution to the quantum tunnelling relaxation of the magnetisation and therefore a slow down of the relaxation time.

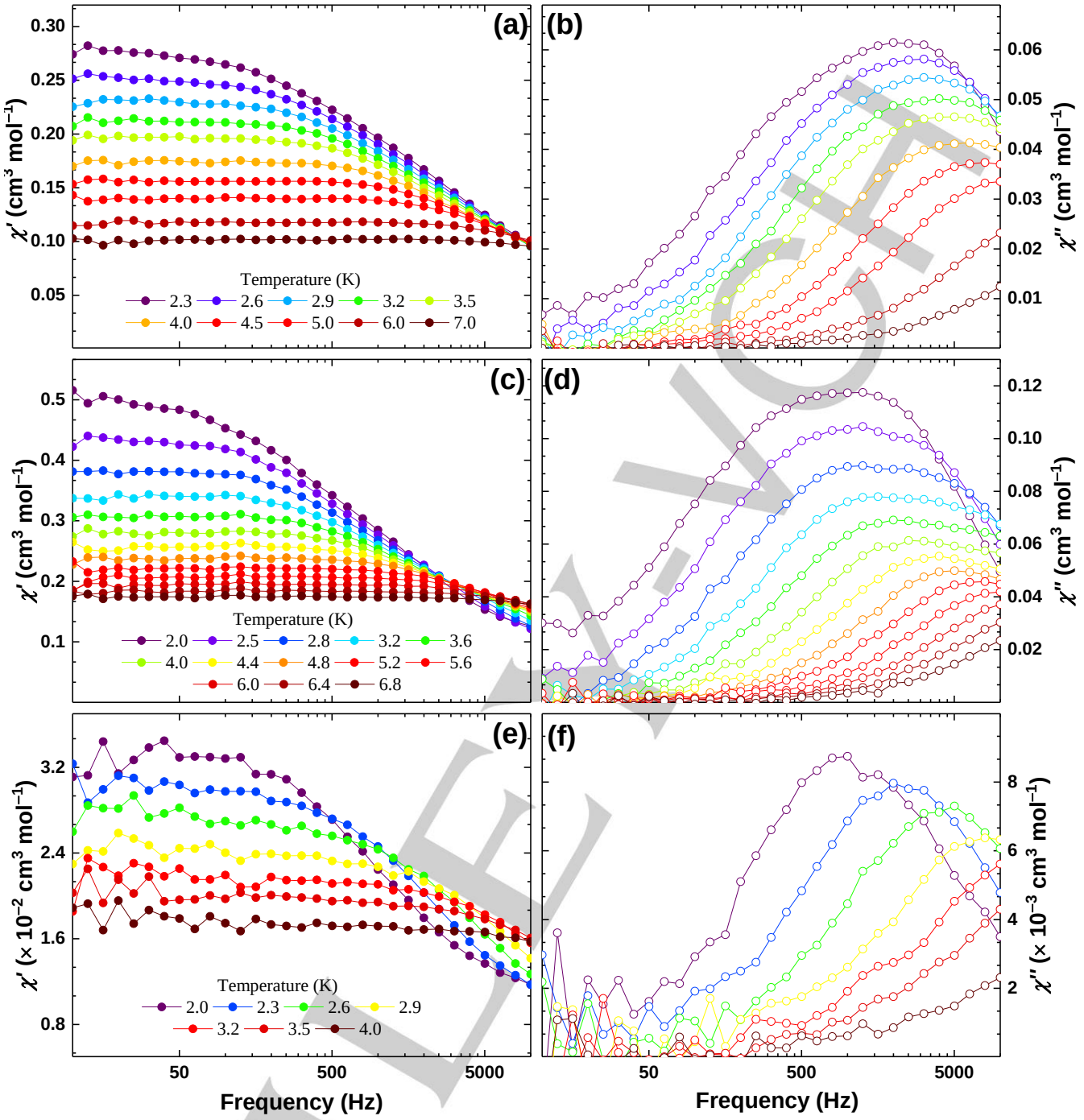

Figure 5. Temperature scan of the magnetic susceptibility for complex **1** at 2600 Oe a) in-phase and b) out-of-phase; complex **3** at 1400 Oe c) in-phase and d) out-of-phase; complex **4** at 2600 Oe e) in-phase and f) out-of-phase.

The major challenge for materials showing SMM behaviour is the loss of the slow magnetic relaxation phenomenon as the temperature is increased. This means that investigations of SMM behaviour cannot be complete without looking at the relationship between the observed slow magnetic relaxation with temperature. A temperature scan between 1.85 K and 10 K using the corresponding optimum field for complexes **1**, **3**, **4**, **6**, **6''**, **8**, and **8''** as determined from field scan gave an insight on the nature of the relaxation dynamics in the systems (Figure 5, 6 and 7). Above 10 K, for all complexes, the relaxation time is far out of the frequency range of the magnetometer and therefore can not be investigated.

The temperature-dependent in-phase and out-of-phase molar susceptibility *vs* frequency plot of **1**, **3**, and **4** obtained using the

optimum field of 2600, 1400, and 2600 Oe respectively are shown in Figure 5. The relaxation dynamics follow the usual trend, showing a peak maximum at 2 K for each case and a corresponding shift to a higher frequency as the temperature is increased. Complexes **1**, **3** and **4** show relaxation peak around 1000 Hz at 2 K. However, complex **4** showed a wider variation in the relaxation dynamics as the temperature is increased. The closer range of relaxation time distribution observed for **1** and **3** as the temperature is decreased could be related to the energy spacing between each degenerate m_j states of the Kramers pairs under ligand-field interaction.[2] In the applied field, **1**, **3** and **5** produce 1, 2 and 3 Kramers pairs leading to a broader distribution of energy spacing for spin reversal as the number of Kramers pairs increases.[2] The electron density from palladium setup a ligand-field perturbation through vibrational mode that interacts with the hybrid orbitals of the lanthanide ions involving the *f*-orbitals and as a result, with the *f*-electrons.[13] As you move from lanthanum across the lanthanide series in the periodic table to samarium (**4**), the effective nuclear charge increases, the tendency to find the electrons in non-degenerate orbitals increases as the free lanthanide ion interacts with the ligand-field and the applied magnetic field to split the Kramers ion's ground state. The electron spins, therefore, begin to relax at slightly different energy leading to the broader distribution in relaxation time between 1000 – 10,000 Hz. This is because the spin-orbit interactions for electrons in different non-degenerate ground state will be different when the Kramers doublets are produced. In a previous report, such slow magnetic relaxation was attributed to the electron density donation from palladium d_{z^2} orbital to hybrid orbitals of the lanthanide.[13] The Pd-Ln bond although not as strong as ordinary covalent or conventional dative bond, such interaction was shown to have favourable implication to the SMM behaviour of such systems. The magnetic property observed for the Kramers ions is unique as it arises from the splitting of the Kramers ions to produce Kramers doublets within which the slow magnetic relaxation is propagated. Cole-Cole model (Eq. 2 and 3) have been used to extract the relaxation time at various temperature.

$$\chi'_m = \chi_{adia} + (\chi_{iso} - \chi_{adia})\frac{1 + (\omega\tau)^{(1-\alpha)}sin\frac{\alpha\pi}{2}}{1 + 2(\omega\tau^{(1-\alpha)}sin\frac{\alpha\pi}{2} + (\omega\tau)^{(2-2\alpha)}} \quad \text{_____} \quad 2$$

$$\chi''_m = (\chi_{iso} - \chi_{adia})\frac{(\omega\tau)^{(1-\alpha)}cos\frac{\alpha\pi}{2}}{1 + 2(\omega\tau)^{(1-\alpha)}sin\frac{\alpha\pi}{2} + (\omega\tau)^{(2-2\alpha)}} \quad \text{_____} \quad 3$$

With χ_{adia} and χ_{iso} the adiabatic and isothermal magnetic susceptibility respectively, τ the relaxation time, χ' and χ'' the in-phase (real) and the out-of-phase (imaginary) magnetic susceptibilities, ω the angular moment and α the distribution of τ. The obtained relaxation times were then fitted by equation 4 (where *A* and *C* are coefficients of direct and Raman process, *H* is applied *dc* field, k_B is Boltzmann constant in cm^{-1}/K, *T* is temperature and *n* and *m* are temperature exponents or scaling factors) to obtain information on the relaxation mechanism.

$$\tau = 1/(A(H^4)T^n + \tau_0{}^{-1}exp(-\frac{U_{eff}}{k_BT}) + CT^m) \quad \text{_____} \quad 4$$

The relaxation processes for **1**, **3** and **4** follow similar pathways of competing Orbach and direct processes (Table 3 and Figure S16) with comparable U_{eff} of 33.53, 41.92 and 18.50 $cm^{-1,}$ respectively. The pre-exponential factor, τ_0, for **1**, **3** and **4** were also determined as 8.91×10^{-9}, 1.43×10^{-9} and 2.06×10^{-9} s respectively. At lower temperature regime, the direct process is dominant and as *T* increases, Orbach process became gradually dominant. According to the Kramers theory, QTM is forbidden for systems with half-integer spin, and the degeneracy is expected to be preserved in the absence of magnetic field. However, a possible hyperfine coupling[60–62] of electronic spin to nuclear spins as well as dipolar coupling[22,63] between molecules could lead to a well pronounced QTM in Kramers ions even in the absence of field leading to an inherent QTM.[64] The absence of QTM demonstrates the efficiency of QTM quenching in our system with an effective direct process to compensate the effect of dipole-dipole coupling which would have otherwise caused spin relaxation via QTM.[64] This is well pronounced in the Orbach – direct relaxation time switch which occurs at a lower temperature of 3 K compare to 4 K for **1** and **3** similar to the Orbach – Raman switch previously reported.[65]

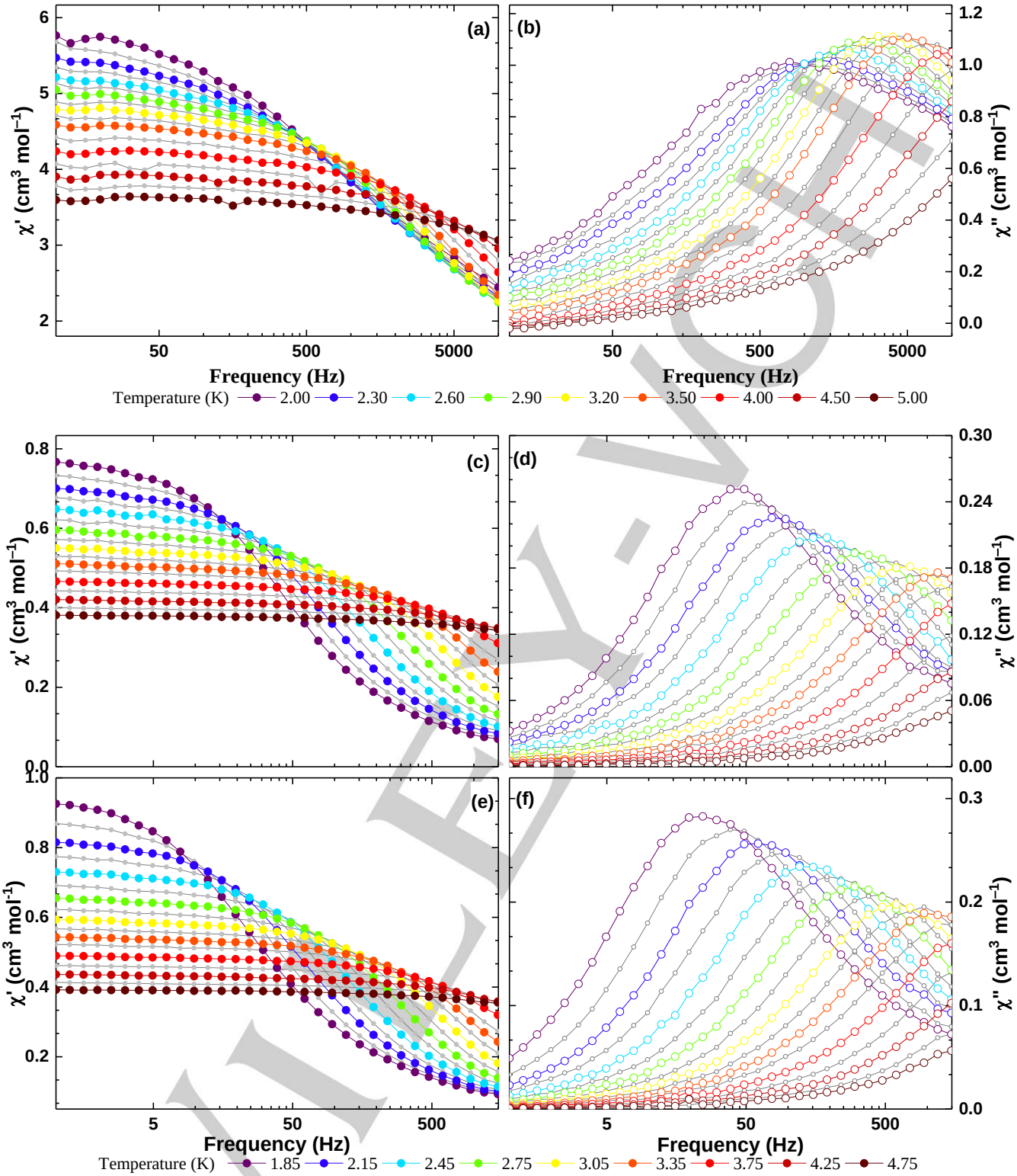

Figure 6. Temperature scan of the magnetic susceptibility for (a) Complex Pd-Dy (6), in-phase at 2000 Oe (b) Complex Pd-Dy (6), out-of-phase at 2000 Oe (c) Complex Pd-Dy-Y (6''), in-phase at 2000 Oe (d) Complex Pd-Dy-Y (6''), out-of-phase at 2000 Oe (e) Complex Pd-Dy-Y (6''), in-phase at 800 Oe (f) Complex Pd-Dy-Y (6''), out-of-phase at 800 Oe.

The temperature-dependent in-phase and out-of-phase molar magnetic susceptibility for **6**, **6''**, **8** and **8''** are shown in Figure 6 and 7. Compound **6** shows a slow magnetic relaxation at high frequencies (between 600 Hz and above 10,000 Hz) under an applied magnetic *dc* field of 2000 Oe. The relaxation times vary widely as the temperature is decreased for complexes **1**, **3** and **4**

mentioned above. Given the higher spin value in complex **6** compared to complexes **1**, **3** and **4**, a diamagnetically diluted sample of **6** (**6"**) was synthesised and used to investigate the role of intermolecular interactions in the relaxation process of complex **6**. The relaxation time became slower in **6"** compare to **6** as a result of the reduction of intermolecular dipole-dipole interactions between the magnetic centres (Dy^{3+}) by dilution with Y^{3+} by 80 %.[55] The slowing down of the relaxation time observed in **6"** compared to **6**, can be attributed to the suppression of the intermolecular dipole-dipole interactions, which enhances QTM. Elimination of the dipole interactions causes the spin to follow an alternative relaxation route than QTM leading to the observed SMM behaviour.[36,50] The τ_0 in **6"** (1.46×10^{-7} s) at the same field of 2000 Oe as in **6** (1.17×10^{-10} s) became even slower confirming the improved slow magnetic relaxation with diamagnetic dilution. To further quantify the effect of the field on the relaxation dynamics of **6"** we carried out another temperature scan for **6"** under a magnetic field of 800 Oe. We observed a faster Orbach process for the case of 800 Oe compares to 2000 Oe. The relaxation mechanism for complex **6"** under 800 Oe cannot be clearly determined from equation 4 and relaxation time *versus T*. A combination of Raman with Orbach or direct, depending on the model chosen, can reproduce the experimental data.

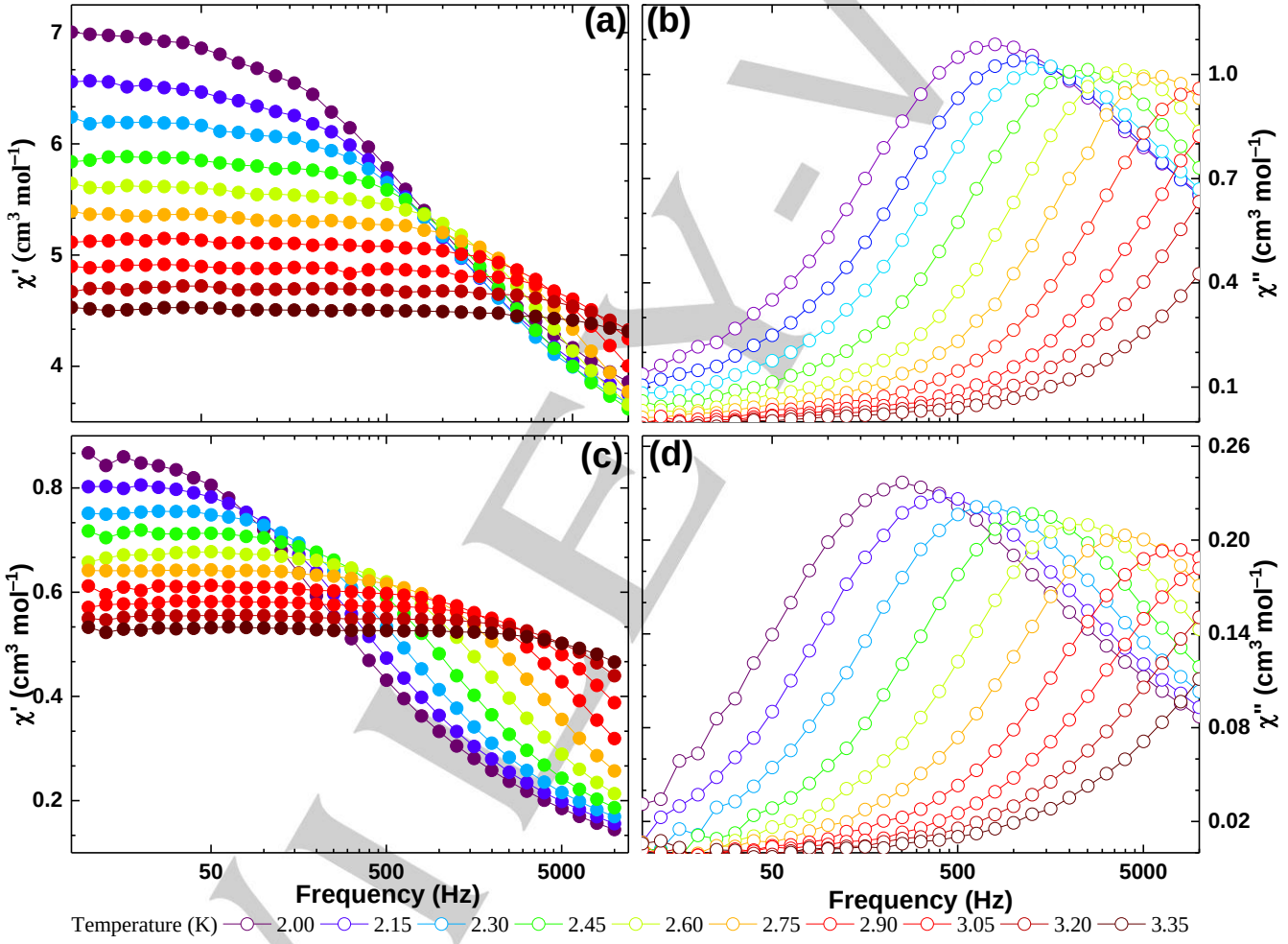

Figure 7. Temperature scan of the magnetic susceptibility for (a) Complex Pd-Er (8), in-phase at 800 Oe (b) Complex Pd-Er (8), out-of-phase at 800 Oe (c) Complex Pd-Er-Y (8"), in-phase at 600 Oe (d) Complex Pd-Er-Y (8"), out-of-phase at 600 Oe.

Similarly, slow magnetic relaxation of complexes **8** and **8"** (Figure 7) at the optimum magnetic field of 800 Oe in the *T* range 2 – 5 K was measured. The diamagnetically diluted sample **8"** showed a slower magnetic relaxation time and more widely spaced relaxation time as the temperature is decreased, due to increased probability of electron spin been found in non-degenerate sublevels than in **1**, **3**, **4**, and **6**.

Table 3. Relaxation parameters for **1, 3, 4, 6, 6'', 8,** and **8''** extracted by fitting the relaxation time at various temperature Caption.

Complex	H / Oe	A /Oe^{-4}s^{-1}K^{-n}	n	U_{eff}/cm	τ_0 /s	C /s^{-1} K^{-m}	m	Adj. R-Square
Pd-Ce (1)	2600	6.24×10^{-11}	1.70	33.53	8.91×10^{-9}	-	-	0.996
Pd-Nd(3)	1400	3.36×10^{-10}	2	41.92	1.43×10^{-9}	-	-	0.997
Pd-Sm(4)	2600	3.59×10^{-11}	2	18.50	2.06×10^{-9}	-	-	0.988
Pd-Dy(6)	2000	1.22×10^{-10}	2	33.19	1.17×10^{-10}	-	-	0.996
Pd-Dy-Y(6'')	2000	5.40×10^{-12}	2	16.01	1.46×10^{-7}	-	-	0.998
Pd-Dy-Y(6'')	800	7.59×10^{-11}	1.59	-	-	1.50	7	0.999
Pd-Dy-Y(6'')	800	-	-	24.30	1.06×10^{-8}	6.58	5.44	0.999
Pd-Er(8)	800	3.73×10^{-9}	2	22.24	3.01×10^{-10}	-	-	0.997
Pd-Er-Y(8'')	600	3.63×10^{-9}	2	20.83	8.10×10^{-10}	-	-	0.998
Pd-Gd(>10 Hz)[13]	3000	1.01×10^{-10}	2	20.71	1.03×10^{-6}	-	-	-
Pd-Gd(<10Hz)[13]	3000	-	-	5.10	0.06	-	-	-
Processes	Direct			Orbach		Raman		

The data of **6**, **6''**, **8** and **8''** were analysed using the Cole-Cole model (equations 2 and 3) to extract the relaxation times at different temperature (Figure S16, S17 and S18) and determine the relaxation mechanism (Table 3). Both Orbach and direct processes compete. We determined U_{eff} of 33.19, 16.01 (at 2000 Oe), 24.30 (at 800 Oe), 22.24, and 20.83 cm^{-1} for **6**, **6''**, **8** and **8''** respectively. An increased U_{eff} value for **6** at 2000 Oe compare to **6''** measured at the same field contrast the τ_0 value as **6** shows a faster τ_0 of 1.17×10^{-10} s whereas **6''** measured at 2000 Oe shows a slower process of 1.46×10^{-7} s. The discrepancy was attributed to an energy barrier created in the presence of intramolecular dipole-dipole interaction which promotes the spin relaxation via the direct process (1.22×10^{-10} s^{-1} K^{-3} for **6**) rather than an Orbach pathway.

The same trend was observed for complexes **8** and **8''** (Table 3) which also showed a slightly faster relaxation for complex **8** despite the higher U_{eff} of 22.24 cm^{-1} for complex **8** compare to 20.83 for complex **8''**. The persistence and improved slow magnetic relaxation for the diamagnetically diluted samples confirm that the observed magnetic behaviour is intrinsic and has a molecular origin. The relaxation dynamics of SMM materials has been shown to occur by allowing electron spins to relax between the ground states and one slightly excited state compared to the ground state. However, the determined U_{eff} for all reported samples is way below any know energy difference between the ground state and the first excited state of expected high-performing lanthanide-based SMM that could be used as a qubit.[66] The only valid explanation for the observed spin reversal is either the splitting of the m_j levels or the anharmonic phonon interaction with the electron spins.[67] The observed energy is more close to the vibrational energy level than that required to excite electrons. The various Pd-O and Ln-O molecular bonds, as well as the Pd-Ln vibrational modes, interact with the spins rather than with the crystal lattice as observed in vanadium-based molecular qubits.[59] The role of the molecular vibrational modes in the slow magnetic relaxation of the Kramers ions across the lanthanide series is in agreement with the observed Orbach mechanism which is mostly moderated by local vibrations.[2]

The ligand field created around the lanthanide complexes splits the atomic *J*-multiplets into several components depending on the number of electrons present. When this splitting takes place, Kramers ions produce doubly degenerate pairs (Kramers doublet) while non-Kramers produces non-degenerate sets in the absence of a strictly axial crystal field symmetry. In previously reported Pt-Ln system,[9,12] slow magnetic relaxation even for the non-Kramers ions like terbium and erbium was observed. This contrasts with the unique trend observed in this study for Pd-Ln counterparts where all non-Kramers doublets do not show slow magnetic

relaxation while all Kramer ions do. The contrast stemmed from the fact that the axial perturbation occasioned by the Pd-Ln vibrational modes was not strong enough to create a bistable state in non-Kramers Pd-Ln systems. [2,38,39,67] The implication is a possible minimal energy splitting of a mixed state for Pd-Ln system which was evident in the MO shown in Figure 2 with *s*- and *f*-orbital mixing. The Pt-Ln counterpart showed slow magnetic relaxation because a bistable state was generated as a result of the strong Pt-Ln axial crystal field symmetry. This is in agreement with stronger electron density donation from Pt $5d_{z^2}$ to the lanthanide ion due to the more radially extended nature of $5d_{z^2}$ over $4d_{z^2}$.[39] Long *et. al*[7] had argued that electron distribution that guarantees more prolate (e.g. Er^{3+}) or more oblate (e.g. Dy^{3+}) would enhance the magnetic anisotropy and hence better SMM behaviour. However, we see that the magnetic anisotropy alone is not the only primary consideration for our systems. Irrespective of whether we have an oblate or prolate quadrupole moment approximation, slow magnetic relaxation was only observed for all lanthanide Kramers ions of our complexes. By comparison with previous reports, we conclude that a robust axial crystal field symmetry is required to observe SMM behavior in non-Kramers ion.

Conclusion

For the first time, we show a unique and complete periodicity in the slow magnetic relaxation of isostructural lanthanide-based complexes spanning the entire lanthanide series. We report the first samarium-based complex exhibiting slow magnetic relaxation and discussed how strong axial crystal field symmetry could combine with other factors like splitting of Kramers doublets to determine whether or not a slow magnetic relaxation can be observed and reaffirm the effect of electron density donation on the SMM behaviour of molecular magnets. The electronic and magnetic properties of the complete lanthanide series of the isostructural acetato bridged heterotetranuclear Pd-Ln complexes showed an alternance of the slow magnetic relaxation characteristic of SMM behaviour moving from Ce to Yb in which all complexes involving non-Kramers ions do not show any SMM behaviour, whereas complexes involving Kramers ions show slow magnetic relaxation. It was occasioned by the electron density donation which set up axial perturbation that causes the splitting of the Kramers ions, allowing the spin to relax slowly through an energy barrier. Comparison with previously reported Pt-Ln system showed that the magnitude of the axial ligand field is necessary to allow observation of SMM behaviour in non-Kramers lanthanide-based systems, a property that Pt displays far better than Pd due to a more radially extended $5d_{z^2}$ orbital of Pt compare to $4d_{z^2}$ of Pd. It was observed that the distribution of slow magnetic relaxation across the lanthanide series for the Kramers ions varies considerably as the number of *f*-electrons increases due to the increased propensity to have electron spin relaxing across non-degenerate sub-levels. We think that this effect also has implication on the SMM behaviour across the lanthanide series with increasing effective nuclear charge which also has consequences on the overall electronic structure. Our study is a holistic review of a family of tetranuclear heterometallic complexes involving the lanthanide series. It is the first holistic study of a complete lanthanide series on slow magnetic relaxation. This study has become significant to understand how SMM behaviour varies across the lanthanide series and seek to give a guide on the variation of SMM property across the series. It was interesting to see that the uncommon lanthanide ions (especially complexes **1**, **3** and **4**) show much slower magnetic relaxation compare to common SMM ions (complexes **6** and **8**). Our results also illustrate the importance of a rigid framework which has helped to maintain a high level of both axiality and geometric similarities along the series. This rarely happens among the lanthanide in which early members usually show different structure and coordination when compared with late members for the same organic ligand. We show that the neglected lanthanide ions need to be explored as much as possible to drive the field of SMM further.

Acknowledgements

This work was partially supported by the CREST, JST Grant number JPMJCR12L3. Professor M. Yamashita thanks the support by the 111 project (B18030) from China. A.J.W.T. thanks the Royal Society for a University Research Fellowship (UF110161)

Keywords: electronic structure • single-molecule magnets • heterometallic lanthanide • theoretical calculation for Kramers and Non-Kramers ion • crystal field and ferromagnetic coupling

ORCID

David Chukwuma Izuogu: 0000-0002-1497-2308
Takefumi Yoshida: 0000-0003-3479-7890
Goulven Cosquer: 0000-0003-2692-1230
Alex J. W. Thom: 0000-0002-2417-7869
Masahiro Yamashita: 0000-0001-8184-4587

Additional information

Supplementary information is available in the online version of the paper.

Competing financial interests

The authors declare no competing financial interests.

References

(1) Tejada, J.; Chudnovsky, E. M.; Barco, E. del; Hernandez, J. M.; Spiller, T. P. Magnetic Qubits as Hardware for Quantum Computers. *Nanotechnology* **2001**, *12* (2), 181–186. https://doi.org/10.1088/0957-4484/12/2/323.

(2) Goodwin, C. A. P.; Ortu, F.; Reta, D.; Chilton, N. F.; Mills, D. P. Molecular Magnetic Hysteresis at 60 Kelvin in Dysprosocenium. *Nature* **2017**, *548* (7668), 439–442. https://doi.org/10.1038/nature23447.

(3) Guo, F.-S.; Day, B. M.; Chen, Y.-C.; Tong, M.-L.; Mansikkamäki, A.; Layfield, R. A. Magnetic Hysteresis up to 80 Kelvin in a Dysprosium Metallocene Single-Molecule Magnet. *Science (80-.).* **2018**, *362* (6421), 1400–1403. https://doi.org/10.1126/science.aav0652.

(4) Randall McClain, K.; Gould, C. A.; Chakarawet, K.; Teat, S. J.; Groshens, T. J.; Long, J. R.; Harvey, B. G. High-Temperature Magnetic Blocking and Magneto-Structural Correlations in a Series of Dysprosium(Iii) Metallocenium Single-Molecule Magnets. *Chem. Sci.* **2018**, *9* (45), 8492–8503. https://doi.org/10.1039/c8sc03907k.

(5) Frost, J. M.; Harriman, K. L. M.; Murugesu, M. The Rise of 3-d Single-Ion Magnets in Molecular Magnetism: Towards Materials from Molecules? *Chem. Sci.* **2016**, *7* (4), 2470–2491. https://doi.org/10.1039/C5SC03224E.

(6) Woodruff, D. N.; Winpenny, R. E. P.; Layfield, R. A. Lanthanide Single-Molecule Magnets. *Chem. Rev.* **2013**, *113* (7), 5110–5148. https://doi.org/10.1021/cr400018q.

(7) Rinehart, J. D.; Long, J. R. Exploiting Single-Ion Anisotropy in the Design of f-Element Single-Molecule Magnets. *Chem. Sci.* **2011**, *2*, 2078–2085. https://doi.org/10.1039/c1sc00513h.

(8) Neese, F.; Pantazis, D. A. What Is Not Required to Make a Single Molecule Magnet. *Faraday Discuss.* **2011**, *148* (0), 229–238. https://doi.org/10.1039/c005256f.

(9) Yoshida, T.; Izougu, D. C.; Iwasawa, D.; Ogata, S.; Hasegawa, M.; Breedlove, B. K.; Cosquer, G.; Wernsdorfer, W.; Yamashita, M. Multiple Magnetic Relaxation Pathways and Dual-Emission Modulated by a Heterometallic Tb-Pt Bonding Environment. *Chem. - A Eur. J.* **2017**, *23* (44), 10527–10531. https://doi.org/10.1002/chem.201702989.

(10) Velkos, G.; Krylov, D. S.; Kirkpatrick, K.; Liu, X.; Spree, L.; Wolter, A. U. B.; Büchner, B.; Dorn, H. C.; Popov, A. A. Giant Exchange Coupling and Field-Induced Slow Relaxation of Magnetization in Gd 2 @C 79 N with a Single-Electron Gd–Gd Bond. *Chem. Commun.* **2018**, *54* (23), 2902–2905. https://doi.org/10.1039/C8CC00112J.

(11) Yoshida, T.; Cosquer, G.; Izuogu, D. C.; Ohtsu, H.; Kawano, M.; Lan, Y.; Wernsdorfer, W.; Nojiri, H.; Breedlove, B. K.; Yamashita, M. Field-Induced Slow Magnetic Relaxation of Gd III Complex with a Pt−Gd Heterometallic Bond. *Chem. - A Eur. J.* **2017**, *23* (19), 4551–4556. https://doi.org/10.1002/chem.201700886.

(12) Yoshida, T.; Izuogu, D. C.; Zhang, H.-T.; Cosquer, G.; Abe, H.; Wernsdorfer, W.; Breedlove, B. K.; Yamashita, M. Ln–Pt Electron Polarization Effects on the Magnetic Relaxation of Heterometallic Ho– and Er–Pt Complexes. *Dalt. Trans.* **2018**. https://doi.org/10.1039/C8DT03338B.

(13) Izuogu, D. C.; Yoshida, T.; Zhang, H.; Cosquer, G.; Katoh, K.; Ogata, S.; Hasegawa, M.; Nojiri, H.; Damjanović, M.; Wernsdorfer, W.; et al. Slow Magnetic Relaxation in a Palladium–Gadolinium Complex Induced by Electron Density Donation from the Palladium Ion. *Chem. - A Eur. J.* **2018**, *24* (37), 9285–9294. https://doi.org/10.1002/chem.201800699.

(14) Goodwin, C. A. P.; Ortu, F.; Reta, D.; Chilton, N. F.; Mills, D. P. Molecular Magnetic Hysteresis at 60 Kelvin in Dysprosocenium. *Nature* **2017**, *548* (7668), 439–442. https://doi.org/10.1038/nature23447.

(15) Norel, L.; Darago, L. E.; Le Guennic, B.; Chakarawet, K.; Gonzalez, M. I.; Olshansky, J. H.; Rigaut, S.; Long, J. R. A Terminal Fluoride Ligand Generates Axial Magnetic Anisotropy in Dysprosium Complexes. *Angew. Chemie Int. Ed.* **2018**, *57* (7), 1933–1938. https://doi.org/10.1002/anie.201712139.

(16) Pugh, T.; Chilton, N. F.; Layfield, R. A. A Low-Symmetry Dysprosium Metallocene Single-Molecule Magnet with a High Anisotropy Barrier. *Angew. Chemie Int. Ed.* **2016**, *55* (37), 11082–11085. https://doi.org/10.1002/anie.201604346.

(17) Mishra, A.; Wernsdorfer, W.; Abboud, K. a; Christou, G. Initial Observation of Magnetization Hysteresis and Quantum Tunneling in Mixed Manganese-Lanthanide Single-Molecule Magnets. *J. Am. Chem. Soc* **2004**, *126* (48), 15648–15649. https://doi.org/10.1021/ja0452727.

(18) Liu, K.; Shi, W.; Cheng, P. Toward Heterometallic Single-Molecule Magnets: Synthetic Strategy, Structures and

Properties of 3d–4f Discrete Complexes. *Coord. Chem. Rev.* **2015**, *289–290*, 74–122. https://doi.org/10.1016/j.ccr.2014.10.004.

(19) Osa, S.; Kido, T.; Matsumoto, N.; Re, N.; Pochaba, A.; Mrozinski, J. A Tetranuclear 3d−4f Single Molecule Magnet: [Cu II LTb III (Hfac) 2] 2. *J. Am. Chem. Soc.* **2004**, *126* (2), 420–421. https://doi.org/10.1021/ja037365e.

(20) Ahmed, N.; Das, C.; Vaidya, S.; Srivastava, A. K.; Langley, S. K.; Murray, K. S.; Shanmugam, M.; Al-Oweini, R.; Sartorel, A.; Bassil, B. S.; et al. Probing the Magnetic and Magnetothermal Properties of M(Ii)–Ln(Iii) Complexes (Where M(Ii) = Ni or Zn; Ln(Iii) = La or Pr or Gd). *Dalt. Trans.* **2014**, *43* (46), 17375–17384. https://doi.org/10.1039/C4DT02360A.

(21) Ruiz, J.; Lorusso, G.; Evangelisti, M.; Brechin, E. K.; Pope, S. J. A.; Colacio, E. Closely-Related Zn II 2 Ln III 2 Complexes (Ln III = Gd, Yb) with Either Magnetic Refrigerant or Luminescent Single-Molecule Magnet Properties. *Inorg. Chem.* **2014**, *53* (7), 3586–3594. https://doi.org/10.1021/ic403097s.

(22) Amjad, A.; Madalan, A. M.; Andruh, M.; Caneschi, A.; Sorace, L. Slow Relaxation of Magnetization in an Isostructural Series of Zinc–Lanthanide Complexes: An Integrated EPR and AC Susceptibility Study. *Chem. - A Eur. J.* **2016**, *22* (36), 12849–12858. https://doi.org/10.1002/chem.201601996.

(23) Long, J. Luminescent Schiff-Base Lanthanide Single-Molecule Magnets: The Association between Optical and Magnetic Properties. *Front. Chem.* **2019**, *7* (FEB), 1–7. https://doi.org/10.3389/fchem.2019.00063.

(24) Goswami, S.; Mondal, A. K.; Konar, S. Nanoscopic Molecular Magnets. *Inorg. Chem. Front.* **2015**, *2* (8), 687–712. https://doi.org/10.1039/C5QI00059A.

(25) Campbell, V. E.; Bolvin, H.; Rivière, E.; Guillot, R.; Wernsdorfer, W.; Mallah, T. Structural and Electronic Dependence of the Single-Molecule- Magnet Behavior of Dysprosium(III) Complexes. *Inorg. Chem.* **2014**, *53*, 2598–2605. https://doi.org/10.1021/ic402950j.

(26) Zhu, J.; Wang, C.; Luan, F.; Liu, T.; Yan, P.; Li, G. Local Coordination Geometry Perturbed β-Diketone Dysprosium Single-Ion Magnets. *Inorg. Chem.* **2014**, *53* (17), 8895–8901. https://doi.org/10.1021/ic500501r.

(27) Singh, S. K.; Gupta, T.; Shanmugam, M.; Rajaraman, G. Unprecedented Magnetic Relaxation via the Fourth Excited State in Low-Coordinate Lanthanide Single-Ion Magnets : A Theoretical Perspective. *Chem. Commun.* **2014**, *50*, 15513–15516. https://doi.org/10.1039/C4CC05522E.

(28) Aubin, S. M. J.; Sun, Z.; Pardi, L.; Krzystek, J.; Folting, K.; Brunel, L.-C.; Rheingold, A. L.; Christou, G.; Hendrickson, D. N. Reduced Anionic Mn 12 Molecules with Half-Integer Ground States as Single-Molecule Magnets. **1999**. https://doi.org/10.1021/ic990613g.

(29) Katoh, K.; Asano, R.; Miura, A.; Horii, Y.; Morita, T.; Breedlove, B. K.; Yamashita, M. Effect of f–f Interactions on Quantum Tunnelling of the Magnetization: Mono- and Dinuclear Dy(Iii) Phthalocyaninato Triple-Decker Single-Molecule Magnets with the Same Octacoordination Environment. *Dalt. Trans.* **2014**, *43* (21), 7716. https://doi.org/10.1039/c4dt00042k.

(30) Katoh, K.; Kajiwara, T.; Nakano, M.; Nakazawa, Y.; Wernsdorfer, W.; Ishikawa, N.; Breedlove, B. K.; Yamashita, M. Magnetic Relaxation of Single-Molecule Magnets in an External Magnetic Field: An Ising Dimer of a Terbium(III)-Phthalocyaninate Triple-Decker Complex. *Chem. - A Eur. J.* **2011**, *17* (1), 117–122. https://doi.org/10.1002/chem.201002026.

(31) Horii, Y.; Katoh, K.; Yasuda, N.; Breedlove, B. K.; Yamashita, M. Effects of f–f Interactions on the Single-Molecule Magnet Properties of Terbium(III)–Phthalocyaninato Quintuple-Decker Complexes. *Inorg. Chem.* **2015**, *54* (7), 3297–3305. https://doi.org/10.1021/ic502951t.

(32) Katoh, K.; Umetsu, K.; Breedlove Brian, K.; Yamashita, M. Magnetic Relaxation Behavior of a Spatially Closed Dysprosium(III) Phthalocyaninato Double-Decker Complex. *Sci. China Chem.* **2012**, *55* (6), 918–925. https://doi.org/10.1007/s11426-012-4615-9.

(33) Wang, H.; Qi, D.; Xie, Z.; Cao, W.; Wang, K.; Shang, H.; Jiang, J. A Sandwich-Type Phthalocyaninato Metal Sextuple-Decker Complex: Synthesis and NLO Properties. *Chem. Commun.* **2013**, *49* (9), 889–891. https://doi.org/10.1039/C2CC38088A.

(34) Wang, H.; Qian, K.; Wang, K.; Bian, Y.; Jiang, J.; Gao, S. Sandwich-Type Tetrakis(Phthalocyaninato) Dysprosium-Cadmium Quadruple-Decker SMM. *Chem. Commun.* **2011**, *47* (34), 9624–9626. https://doi.org/10.1039/c1cc12509e.

(35) Fukuda, T.; Biyajima, T.; Kobayashi, N. A Discrete Quadruple-Decker Phthalocyanine. *J. Am. Chem. Soc.* **2010**, *132* (18), 6278–6279. https://doi.org/10.1021/ja100125e.

(36) Ishikawa, N.; Iino, T.; Kaizu, Y. Interaction between F-Electronic Systems in Dinuclear Lanthanide Complexes with Phthalocyanines. *J. Am. Chem. Soc.* **2002**, *124* (38), 11440–11447. https://doi.org/10.1021/ja027119n.

(37) Yoshida, T.; Cosquer, G.; Izuogu, D. C.; Ohtsu, H.; Kawano, M.; Lan, Y.; Wernsdorfer, W.; Nojiri, H.; Breedlove, B. K.; Yamashita, M. Field-Induced Slow Magnetic Relaxation of GdIII Complex with a Pt−Gd Heterometallic Bond. *Chem. - A Eur. J.* **2017**, *23* (19), 4551–4556. https://doi.org/10.1002/chem.201700886.

(38) Izuogu, D. C.; Yoshida, T.; Zhang, H.; Cosquer, G.; Katoh, K.; Ogata, S.; Hasegawa, M.; Nojiri, H.; Damjanović, M.; Wernsdorfer, W.; et al. Slow Magnetic Relaxation in a Palladium-Gadolinium Complex Induced by Electron Density Donation from the Palladium Ion. *Chem. - A Eur. J.* **2018**, *24* (37), 9285–9294. https://doi.org/10.1002/chem.201800699.

(39) Sørensen, M. A.; Weihe, H.; Vinum, M. G.; Mortensen, J. S.; Doerrer, L. H.; Bendix, J. Imposing High-Symmetry and Tuneable Geometry on Lanthanide Centres with Chelating Pt and Pd Metalloligands. *Chem. Sci.* **2017**, *8*, 3566. https://doi.org/10.1039/c7sc00135e.

(40) Gómez-Coca, S.; Urtizberea, A.; Cremades, E.; Alonso, P. J.; Camón, A.; Ruiz, E.; Luis, F. Origin of Slow Magnetic Relaxation in Kramers Ions with Non-Uniaxial Anisotropy. *Nat. Commun.* **2014**, *5*, 4300. https://doi.org/10.1038/ncomms5300.

(41) Sugita, M.; Ishikawa, N.; Ishikawa, T.; Koshihara, S.; Kaizu, Y. Static Magnetic-Field-Induced Phase Lag in the Magnetization Response of Tris(Dipicolinato)Lanthanides. *Inorg. Chem.* **2006**, *45* (3), 1299–1304. https://doi.org/10.1021/ic051089i.

(42) Zhu, J.; Wang, C.; Luan, F.; Liu, T.; Yan, P.; Li, G. Local Coordination Geometry Perturbed B-Diketone Dysprosium Single-Ion Magnets. *Inorg. Chem.* **2014**, *53* (17), 8895–8901. https://doi.org/10.1021/ic500501r.

(43) Liu, J.-L.; Chen, Y.-C.; Tong, M.-L. Symmetry Strategies for High Performance Lanthanide-Based Single-Molecule Magnets. *Chem. Soc. Rev.* **2018**, *47* (7), 2431–2453. https://doi.org/10.1039/C7CS00266A.

(44) Alonso, P. J. J.; Martinez, J. I.; Martínez, J. I. Magnetic Properties of a Kramers Doublet. An Univocal Bridge between Experimental Results and Theoretical Predictions. *J. Magn. Reson.* **2015**, *255*, 1–14. https://doi.org/10.1016/j.jmr.2015.03.010.

(45) Jiang, S.-D.; Bing-Wu Wang, A.; Gao, S. Applications of Layered Double HydroxidesAdvances in Lanthanide Single-Ion Magnets. *Struct. Bond.* **2015**, *164* (September 2005), 111–142. https://doi.org/10.1007/430_2014_153.

(46) Nefedov, S. E.; Kozitsyna, N. Y.; Vargaftik, M. N.; Moiseev, I. I. Palladium(II)-Rare-Earth Metal(III) Paddlewheel Carboxylate Complexes: Easy Total Acetate to Pivalate Metathesis. *Polyhedron* **2009**, *28* (1), 172–180. https://doi.org/10.1016/j.poly.2008.10.006.

(47) Liddle, S. T.; van Slageren, J. Improving F-Element Single Molecule Magnets. *Chem. Soc. Rev.* **2015**, *44* (19), 6655–6669. https://doi.org/10.1039/c5cs00222b.

(48) Skomski, R. *Simple Models of Magnetism*, First Edit.; Oxford University Press: New York, 2008.

(49) Kahn, O. *Molecular Magnetism*; VCH Publishers, Inc: New York, 1993.

(50) Fukuda, T.; Kuroda, W.; Ishikawa, N. Observation of Long-Range f–f Interactions between Two f-Electronic Systems in Quadruple-Decker Phthalocyanines. *Chem. Commun.* **2011**, *47* (42), 11686. https://doi.org/10.1039/c1cc14657b.

(51) Kajiwara, T. A Holmium(III)-Based Single-Molecule Magnet with Pentagonal-Bipyramidal Geometry. *Angew. Chemie Int. Ed.* **2017**, *56* (38), 11306–11308. https://doi.org/10.1002/anie.201703022.

(52) Pointillart, F.; Cador, O.; Le Guennic, B.; Ouahab, L. Uncommon Lanthanide Ions in Purely 4f Single Molecule Magnets. *Coordination Chemistry Reviews*. Elsevier B.V. September 1, 2017, pp 150–175. https://doi.org/10.1016/j.ccr.2016.12.017.

(53) L. L.S. Melo, L.; P. Castro, G.; M. C. Gonçalves, S. Substantial Intensification of the Quantum Yield of Samarium(III) Complexes by Mixing Ligands: Microwave-Assisted Synthesis and Luminescence Properties. *Inorg. Chem.* **2019**, *58* (5), 3265–3270. https://doi.org/10.1021/acs.inorgchem.8b03340.

(54) Hofmann, A.; Salman, Z. Tuning the Spin Dynamics of Single Molecule Magnets via Dipolar Interactions. *ACS Nano* **2014**, *6* (1), 010. https://doi.org/10.1088/1742-6596/551/1/012055.

(55) Meihaus, K. R.; Rinehart, J. D.; Long, J. R. Dilution-Induced Slow Magnetic Relaxation and Anomalous Hysteresis in Trigonal Prismatic Dysprosium(III) and Uranium(III) Complexes. **2011**. https://doi.org/10.1021/ic201078r.

(56) Harriman, K. L. M.; Murugesu, M. An Organolanthanide Building Block Approach to Single-Molecule Magnets. *Acc. Chem. Res.* **2016**, *49* (6), 1158–1167. https://doi.org/10.1021/acs.accounts.6b00100.

(57) Tesi, L.; Lunghi, A.; Atzori, M.; Lucaccini, E.; Sorace, L.; Totti, F.; Sessoli, R. Giant Spin–Phonon Bottleneck Effects in Evaporable Vanadyl-Based Molecules with Long Spin Coherence. **2016**, *45*. https://doi.org/10.1039/c6dt02559e.

(58) Lunghi, A.; Sanvito, S. Spin-Phonon Relaxation in

Molecular Qubits from First Principles Spin Dynamics. **2019**.

(59) Atzori, M.; Tesi, L.; Benci, S.; Lunghi, A.; Righini, R.; TASCHIN, A.; Torre, R.; Sorace, L.; Sessoli, R. Spin Dynamics and Low Energy Vibrations: Insights from Vanadyl-Based Potential Molecular Qubits. *J. Am. Chem. Soc.* **2017**. https://doi.org/10.1021/jacs.7b01266.

(60) Flores Gonzalez, J.; Pointillart, F.; Cador, O. Hyperfine Coupling and Slow Magnetic Relaxation in Isotopically Enriched DyIII Mononuclear Single-Molecule Magnets. *Inorg. Chem. Front.* **2019**, *6* (4), 1081–1086. https://doi.org/10.1039/c8qi01209a.

(61) Luis, F.; Martínez-Pérez, M. J.; Montero, O.; Coronado, E.; Cardona-Serra, S.; Martí-Gastaldo, C.; Clemente-Juan, J. M.; Sesé, J.; Drung, D.; Schurig, T. Spin-Lattice Relaxation via Quantum Tunneling in an Er3+ -Polyoxometalate Molecular Magnet. *Phys. Rev. B* **2010**, *82* (6), 060403. https://doi.org/10.1103/PhysRevB.82.060403.

(62) Giansiracusa, M. J.; Moreno-Pineda, E.; Hussain, R.; Marx, R.; Martínez Prada, M.; Neugebauer, P.; Al-Badran, S.; Collison, D.; Tuna, F.; van Slageren, J.; et al. Measurement of Magnetic Exchange in Asymmetric Lanthanide Dimetallics: Toward a Transferable Theoretical Framework. *J. Am. Chem. Soc.* **2018**, *140* (7), 2504–2513. https://doi.org/10.1021/jacs.7b10714.

(63) Pointillart, F.; Le Gal, Y.; Golhen, S.; Cador, O.; Ouahab, L. Single-Molecule Magnet Behaviour in a Tetrathiafulvalene-Based Electroactive Antiferromagnetically Coupled Dinuclear Dysprosium(III) Complex. *Chem. - A Eur. J.* **2011**, *17* (37), 10397–10404. https://doi.org/10.1002/chem.201100869.

(64) Sorace, L.; Gatteschi, D. *Lanthanides and Actinides in Molecular Magnetism*; Layfield, R. A., Murugesu, M., Eds.; Wiley-VCH: Weinheim, 2015.

(65) Giansiracusa, M. J.; Kostopoulos, A. K.; Collison, D.; Winpenny, R. E. P.; Chilton, N. F. Correlating Blocking Temperatures with Relaxation Mechanisms in Monometallic Single-Molecule Magnets with High Energy Barriers (U Eff > 600 K). *Chem. Commun.* **2019**, *55* (49), 7025–7028. https://doi.org/10.1039/C9CC02421B.

(66) Ding, Y.-S.; Deng, Y.-F.; Zheng, Y.-Z. The Rise of Single-Ion Magnets as Spin Qubits. *Magnetochemistry* **2016**, *2* (4), 40. https://doi.org/10.3390/magnetochemistry2040040.

(67) Lunghi, A.; Totti, F.; Sessoli, R.; Sanvito, S. The Role of Anharmonic Phonons in Under-Barrier Spin Relaxation of Single Molecule Magnet. *Nat. Commun.* **2017**, *8*, 14620. https://doi.org/10.1038/ncomms14620.

Entry for the Table of Contents

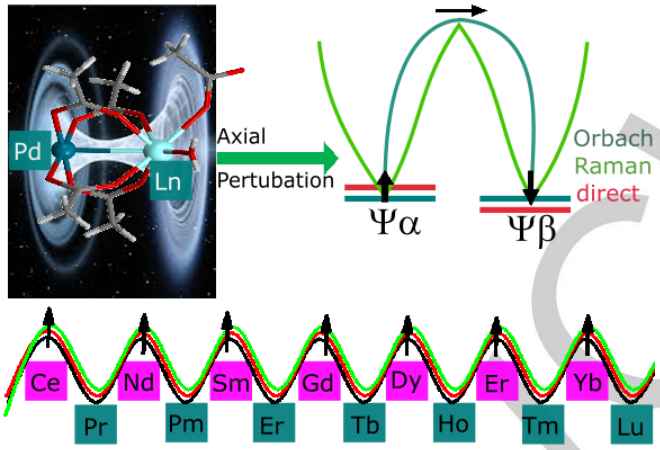

Text for Table of Contents: The dynamics of single-molecule magnets (SMMs) behaviour modulated by heterometallic bonding interaction axial to the lanthanide ion was investigated holistically for all lanthanide ions of the lanthanide series using series of experimental and theoretical methods. We observed a unique trend with divergence depending on whether the ion is Kramers or non-Kramers across the period. We give insight on what is responsible and affirm a new consideration for SMM design.

Institute and/or researcher Twitter usernames: @Cambridge_uni, @ChemCambridge, @ThomGroupCam, @Chucksty